Identification of Soft Tissue-Mimicking Materials and Application in the Characterization of Sensors for Lung Sounds

Paolo La Torraca, Ludovico Ausiello, Giorgio Zucchi, Angelo Farina and Fabrizio Pancaldi, *Member, IEEE*

***Abstract*— Early diagnosis of pulmonary implications is fundamental for the treatment of several diseases, such as idiopathic pulmonary fibrosis, rheumatoid arthritis, connective tissue diseases and interstitial pneumonia secondary to COVID-19 among the many. Recent studies prove that a wide class of pulmonary diseases can be early detected by auscultation and suitably developed algorithms for the analysis of lung sounds. Indeed, the technical characteristics of sensors have an impact on the quality of the acquired lung sounds. The availability of a fair and quantitative approach to sensors' comparison is a prerequisite for the development of new diagnostic tools. In this work the problem of a fair comparison between sensors for lung sounds is decoupled into two steps. The first part of this study is devoted to the identification of a synthetic material capable of mimicking the acoustic behavior of human soft tissues; this material is then adopted as a reference. In the second part, the *standard skin* is exploited to quantitatively compare several types of sensors in terms of noise floor and sensitivity. The proposed methodology leads to reproducible results and allows to consider sensors of different nature, e.g. laryngophone, electret microphone, digital MEMS microphone, mechanical phonendoscope and electronic phonendoscope. Finally, the experimental results are interpreted under the new perspective of equivalent sensitivity and some important guidelines for the design of new sensors are provided. These guidelines could represent the starting point for improving the devices for acquisition of lung sounds.**

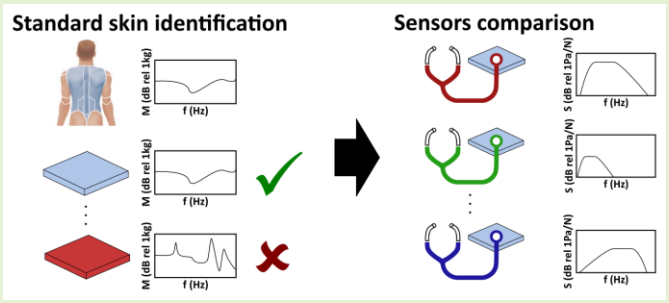

***Index Terms*—Acoustic sensor, human soft tissues, lung sounds, sensor bandwidth, sensor sensitivity.**

I. Introduction

ACOUSTIC information retrieved via digital stethoscopes or equivalent sensors has been used for a plethora of applications, from continuous health monitoring, to automatic recognition and identification of cardiac patterns, to person identification algorithms [1]–[3]. Recently, various studies have proved the effectiveness of electronic phonendoscopes and suitably developed software in the early detection of pulmonary fibrosis and interstitial lung diseases [4]–[6].

Acoustics of stethoscopes and their performance as sensors have been studied for more than 50 years, with seminal articles dating as early as 1966 [7]. Subsequent investigations [8]–[11] consolidated the knowledge that the usable information which can be actually retrieved through a stethoscope is limited to 2 kHz [12], even if Ertel and colleagues measured frequency responses of stethoscopes exceeding 3 kHz of bandwidth [7].

On the one hand, the structure generating the pulmonary sounds is of particular interest for physicians. However, on the other hand, the propagation inside the lung and through the human soft tissues, together with the limitations of the acquisition tool (e.g. a mechano-acoustic stethoscope) contribute to constraint the frequency response of the observed phenomenon and affect the related information content accordingly. As a matter of fact, all the studies trying to grasp the actual acoustic bandwidth of lung sounds are limited by the

This paragraph of the first footnote will contain the date on which you submitted your paper for review.

This work has been partially supported by the research fund "Fondo di Ateneo per la Ricerca (FAR) 2016" allocated by the University of Modena and Reggio Emilia (Italy).

Fabrizio Pancaldi, and Paolo La Torraca are with the University of Modena and Reggio Emilia, Department of Sciences and Methods for Engineering, via Amendola 2, 42122 - Reggio Emilia, Italy (email: fabrizio.pancaldi@unimore.it; paolo.latorraca@unimore.it). Fabrizio Pancaldi is also with the Artificial Intelligence Research and Innovation Center (AIRI), Via Pietro Vivarelli 10, 41125 - Modena, Italy.

Giorgio Zucchi is with the FMB, Marco Biagi Foundation, University of Modena and Reggio Emilia, Largo Marco Biagi 10, 41121 Modena, Italy (email: giorgio.zucchi@unimore.it).

Ludovico Ausiello is with the University of Portsmouth, School of Energy and Electronic Engineering Anglesea Building, Anglesea Road, Portsmouth, UK, (email: Ludovico.ausiello@port.ac.uk). Ludovico Ausiello is also with Solent University Southampton, Media Technology Group – Audio and Acoustics, East Park Terrace, Southampton.

Angelo Farina is with the University of Parma, Department of Engineering and Architecture, Parco Area delle Scienze 181/A, 43124 – Parma, Italy. He also teaches in the Advanced Course on Sound Engineering at the University of Modena and Reggio Emilia, Italy.

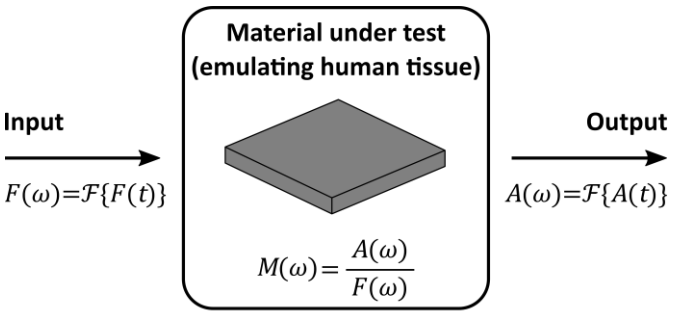

Fig. 1. Block diagram illustrating the system considered for the evaluation of the apparent mass M(ω) of the material under investigation.

Fig. 2. Experimental setup for the apparent mass characterization of the *standard skin* candidates. A sample of the material under test is excited with a Brüel & Kjær 8202 impact hammer, equipped with a Brüel & Kjær 8200 force transducer and a Brüel & Kjær 4368 accelerometer. The transducers are conditioned using two Brüel & Kjær 2635 charge amplifiers. The resulting voltage signals are simultaneously acquired using a Zoom H4n recorder.

intrinsic difficulty of decoupling the pulmonary murmur from the artefacts superimposed to it by the acquisition system. Few works have tried to fill this gap. Some stethoscopes have been characterized and compared in terms of bandwidth on the basis of the acoustic coupling provided by headphones [11]. Other studies have been devoted to the modeling of wave propagation inside the lungs [8], [13].

The scope of this work is twofold. Firstly, we present an experimental method to characterize and identify synthetic material mimicking the mechano-acoustic behavior of the dorsum (back) of the human thoracic cavity. Both the synthetic

$$M(\omega) = \frac{F(\omega)}{A(\omega)} \qquad (1)$$

materials and the human soft tissues are characterized in terms of apparent mass, which is equivalent to the mechanical impedance. We have characterized 25 acoustic materials through a robust measurement method [14], and then we have drawn up a ranking in terms of similarity to the human soft tissues of the dorsum. The best materials have been elected to, which will become the reference benchmark with whom all subsequent measurements of this article will be drawn. In the second part of the study, the is used to assess and compare a large set of sensors, namely mechanical phonendoscopes (MPs), electronic phonendoscopes (EPs), laryngophones, accelerometers and MEMS microphones. To the best of our knowledge, this work represents the first approach to a repeatable, objective and quantitative comparison of sensors for lung sounds. This comes from the fact that while human tissue (even only for the dorsum) shows a variety of responses that needs averaging, the *standard skin* is a completely characterized material, and, equally important, it is easy to source. This will offer all sensors manufacturers and researchers a solid repeatable platform to perform their future studies and comparisons. In a sense, our contribution can be interpreted as an extension of the original intent of Ertel et al. to create a *standard ear* suitable to quantitatively select the best auscultation tools available at the time [7].

The remaining of this paper is organized as follows. The definitions of apparent mass and mechano-acoustic impedance are given in Section II, where also the measurement setup and the metrics adopted to identify the synthetic *standard skin* are described in detail. The approach to the performance comparison of the considered sensors is presented in Section III. Numerical and experimental results are shown in Section IV. These results are discussed and commented on in Section V, where guidelines for future sensor design are also provided in the light of the retrieved data and of electro-acoustic design criteria. Finally, conclusions are summarized in Section VI.

II. Materials with vibro-acoustic behavior similar to human tissues: the *standard skin*

The system considered for the characterization of the materials is shown in Figure 1: the material under test is excited by a force F(t) and responds with an acceleration A(t). In this framework, a material is characterized by its apparent mass (or inertance) M(ω) [15]:
where ω=2πf is the angular frequency associated to the frequency f, F(ω) is the Fourier transform of the excitation force F(t), i.e. the input of the system, and A(ω) is the Fourier transform of the resulting acceleration A(t), i.e. the output of the system.

For readers unfamiliar to vibrational analysis, we remind that the apparent mass M(ω) of a material is related to its mechanical impedance $Z_M(\omega)$ and its acoustic impedance $Z_A(\omega)$:

$$M(\omega) = \frac{1}{j\omega}\frac{F(\omega)}{V(\omega)} = \frac{1}{j\omega}Z_M(\omega) = \frac{1}{j\omega}S^2 Z_A(\omega) \qquad (2)$$

where V(ω) is the Fourier transform of the velocity v(t) resulting from the force excitation, and S is the reference surface for the measurement of the acoustic impedance [16].

The rationale behind this first part of our study consists of identifying a set of materials characterized by an apparent mass M(ω) as close as possible to human tissues', since the filtering effects on propagating mechano-acoustic waves are similar. We refer to this class of materials as *standard skins*. Once one (or more) material were found, we could then focus on the comparisons of the sensors, without the necessity to perform any other tests on humans, thus greatly reducing the complexity of future studies.

The experimental setup for the characterization of the panels is depicted in Figure 2. A sample of the material under test was firmly attached to a rigid surface and excited with a Brüel & Kjær 8202 impact hammer, equipped with a Brüel & Kjær 8200 force transducer and a Brüel & Kjær 4368 accelerometer. The co-location of the force and acceleration sensors on the hammer head enabled the precise and simultaneous acquisition of the input force F(t) and the resulting acceleration output A(t) of the material under test. The transducers were conditioned using two Brüel & Kjær 2635 charge amplifiers. The resulting voltage

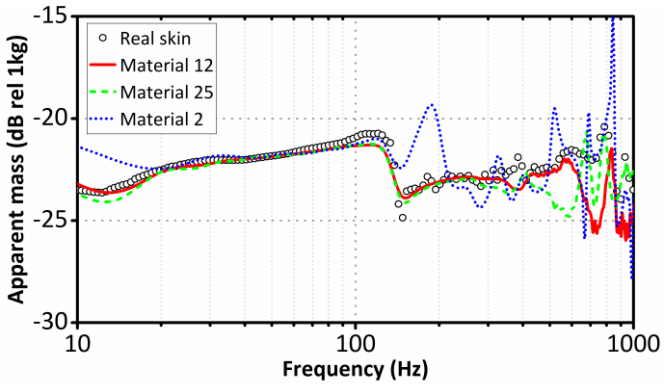

Fig. 3. Comparisons between the measured apparent mass of different materials: real skin (black circles), material 12 (solid red line), material 25 (dashed green line), and material 2 (dotted blue line). Material 12 and material 25 show a good match with the real skin. Conversely, Material 2 shows significant fluctuations not exhibited by the real skin. For more information on the materials, see Appendix A.

signals were simultaneously acquired using a Zoom H4n recorder.

The collected signals were then post-processed in MATLAB with the support of the ITA-Toolbox [16]. The Discrete Fourier Transform (DFT) of the acquired signals is firstly computed, leading to the input force DFT $F(\omega_i)$ and the output acceleration DFT $A(\omega_i)$, where ω_i is the discrete angular frequency resulting from the signals discretization. Each DFT has length N=96000. The apparent mass DFT $M(\omega_i)$ is then computed according to Eq.(1).

The same experimental setup was used in the past for the *in vivo* characterization of the real skin. Measurements were previously collected in a database which was used for this work. The focus was on the human dorsum area, which is of particular interest for phonendoscopic analysis. The database contained apparent masses recorded multiple times in different locations within such an area, taken from different subjects. Accordingly, the value later used as a reference to represent the *in vivo* skin is in fact the pool average of all the collected data, which allowed accounting for the physiological variations of different subjects.

The synthetic materials encompassed in this study are readily available off-the-shelf multi-layered panels normally used in building acoustics [17]. The complete list can be found in Appendix A. In order to select the best synthetic materials, their apparent mass were compared to that of the averaged real skin described above. The apparent mass of three remarkable materials is shown in Figure 3; the real skin is also reported for comparison.

TABLE I
EVALUATION METRICS FOR THE IDENTIFICATION OF THE BEST MATERIALS

Material	MAPE	Material	MSE ($\times 10^6$)
25	**7.56**	**25**	**33.28**
12	**9.61**	**12**	**46.08**
1	9.69	7	59.07
8	10.16	3	60.19
7	10.56	15	65.18
3	11.04	8	65.87
5	11.54	1	67.52
15	11.57	9	86.70
9	12.14	5	97.01
11	12.45	11	103.1

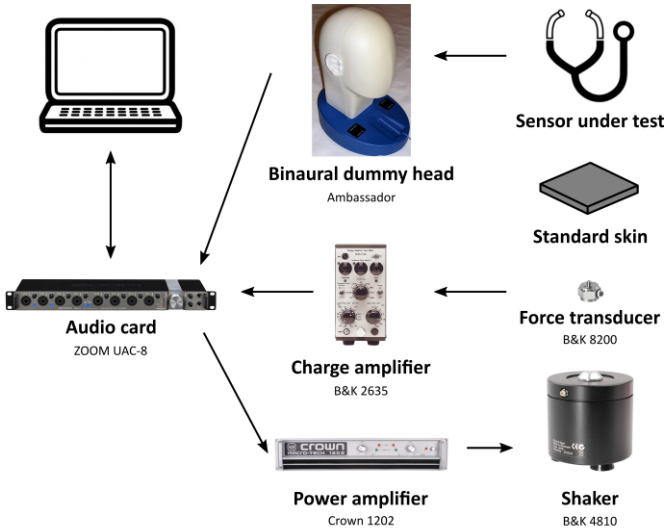

Fig. 4. Experimental setup for the characterization of the sensors for phonendoscopic applications. A PC and a Zoom UAC-8 audio interface are used to simultaneously excite the standard skin and to acquire the signals of interest. The stimulus signal is amplified by a Crown 1202 amplifier and applied to a Brüel & Kjær 4810 shaker equipped with a Brüel & Kjær 8200 force transducer, conditioned with a Brüel & Kjær 2635 charge amplifier. The standard skin is firmly attached to the shaker axis. The sensor under test is attached on top of the standard skin. The signals produced by the sensor are routed to an Ambassador binaural dummy head, either directly or by Sennheiser IE 40 PRO headphones.

Firstly, it is worth pointing out that the bandwidth of the measured data is roughly limited to 1kHz; this is mainly entailed by the intrinsic elasticity of the tested materials and to the real skin considered as reference. The soft tip of the impact hammer might also have a role. Material 25 (SUPERGRAN, mm. 5) and Material 12 (SUPERFINE, mm. 8+3) show a good match with the real skin at low frequencies and just some fluctuations in the highest part of the spectrum. Conversely, Material 2 (MANTOPHON BIT mm. 5+4+5) presents a substantially different apparent mass profile with respect to real skin, thus suggesting that sound propagation and filtering effects would be also significantly different.

To select the best candidates to become standard skin, two performance metrics were used: the Mean Absolute Percentage Error (MAPE) and the Mean Squared Error (MSE) of the materials apparent mass with respect to the real skin one.

In this framework, the MAPE of the materials' apparent mass is defined as:

$$MAPE = \frac{1}{N}\sum_{i=1}^{N}\left|\frac{M_{MAT}(\omega_i) - M_{SKIN}(\omega_i)}{M_{MAT}(\omega_i)}\right| \qquad (3)$$

where M_{MAT} and M_{SKIN} are the apparent mass of the material under test and of the real skin, respectively. Similarly, the MSE of the materials' apparent mass is defined as:

$$MSE = \frac{1}{N}\sum_{i=1}^{N}|M_{MAT}(\omega_i) - M_{SKIN}(\omega_i)|^2 \qquad (4)$$

The MAPE and the MSE of the best ranked materials are shown in Table I. Experimental evidence indicates that the best matching to the real skin is achieved by material 12 and material 25. Accordingly, these materials will be employed as standard skins in the remainder of the work.

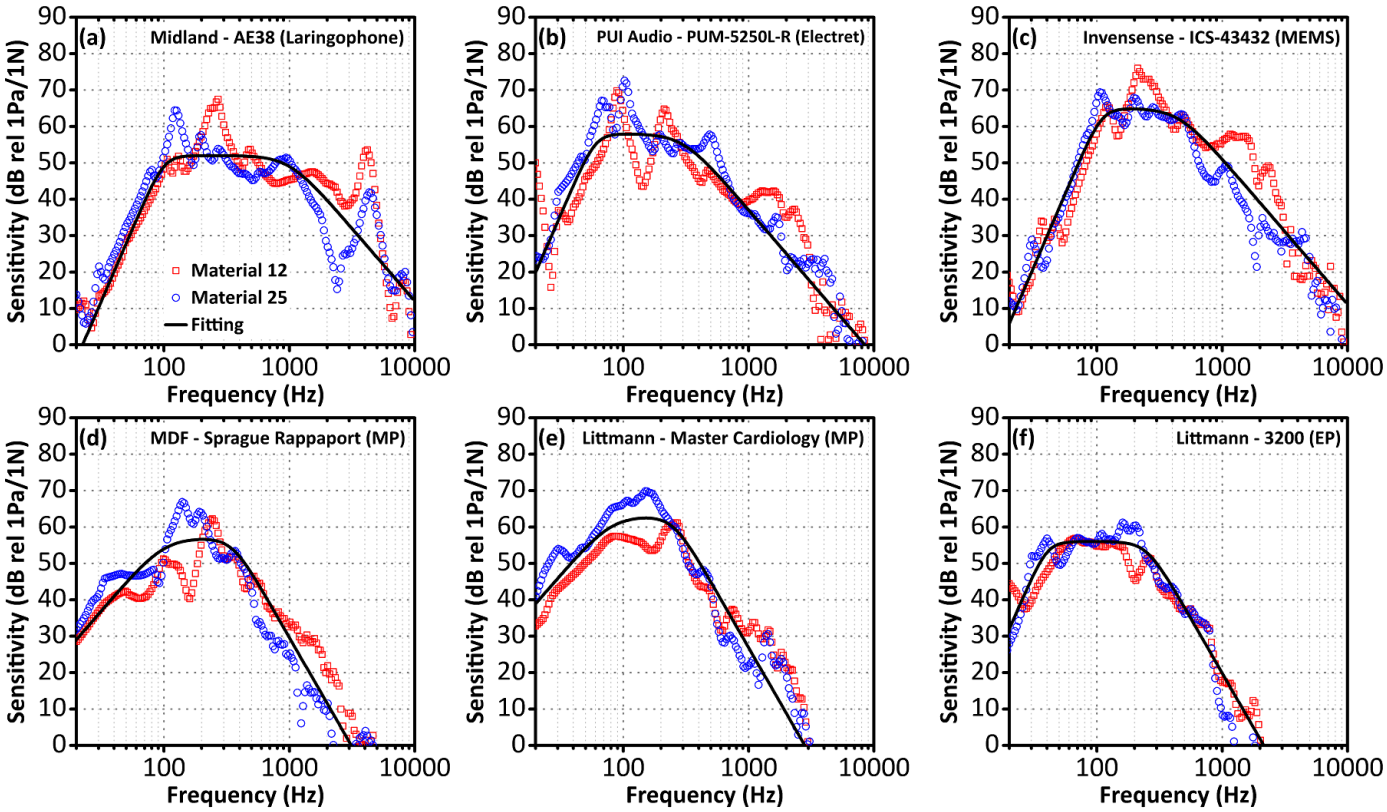

Fig. 5. Experimental sensitivity of the tested sensors, expressed in dB relative to 1Pa/N and measured at 50 dB SPL (A weighted) noise floor. For each sensor, the sensitivity has been measured using both material 12 (red squares) and material 25 (blue circles) as standard skin. The sensors exhibit an overall band-pass behavior, with clearly visible cut-off frequencies. Spurious resonance effects are also detected. The experimental sensitivities are fitted with Butterworth band-pass filters (solid black lines), highlighting the pass-band magnitude, cut-off frequencies and -3dB bandwidth of sensors.

III. Methodology and Measurement Setup for Sensors Comparison

The second part of our study requires an experimental setup to compare a large set of sensors using the fully characterized standard skins. This will be presented in this Section. Moreover, a performance criterion is proposed to draw up a ranking of sensors.

The experimental setup for the characterization of the sensors is depicted in Fig. 4. It is worth pointing out that the considered transducers belong to different classes. Thus, subtle changes have been introduced to each measurement chain in order to yield congruent signals for a fair comparison.

A PC and a Zoom UAC-8 audio interface were used to both excite the standard skin and to acquire the signals of interest.

TABLE II
Summary of the Characterized Sensors

Manufacturer	Model	Technology
Midland	AE38	Laryngophone
PUI Audio	PUM-5250L-R	Electret microphone, mounted on a chest piece
Invensense	ICS-43432	MEMS microphone
MDF	Sprague Rappaport	Mechanical phonendoscope (MP)
Littmann	Master Cardiology	Mechanical phonendoscope (MP)
Littmann	3200	Electronic phonendoscope (EP)

The stimulus signal was amplified by a Crown 1202 amplifier and applied to a Brüel & Kjær 4810 shaker equipped with a Brüel & Kjær 8200 force transducer. The exciting signal was an Exponential Sine Sweep (ESS) with starting frequency of 10 Hz, ending frequency of 10kHz and time support of 20 seconds [18], [19].

The *standard skin* was firmly attached to the shaker axis, and the sensor under test was attached on top of the standard skin using Bostik Blu Tack. The force transducer was conditioned using a Brüel & Kjær 2635 charge amplifier.

Signals produced by the Device Under Test (DUT) were routed to an Ambassador binaural dummy head. DUTs with an acoustic output (i.e. mechanical and electronic phonendoscopes) were directly placed onto the ears of the binaural dummy head, whereas DUTs providing an electrical outputs (i.e. laryngophone, MEMS, and electret microphone) were connected to high quality in-ear headphones (Sennheiser IE 40 PRO) and coupled with the dummy head. It is worth pointing out that this setup mimics real-life operational conditions for each type of sensors and hence results in a fair comparison. All the output signals returned by the binaural dummy head and the charge amplifier were recorded using the same Zoom audio interface.

The input gain of the channel acquiring the DUTs' output (i.e. the signal coming from the binaural dummy head) was specifically tuned for each DUT characterization in order to set the equivalent acoustic noise floor at 50 dB SPL (A weighted). This allowed for a fair comparison of the different DUTs based

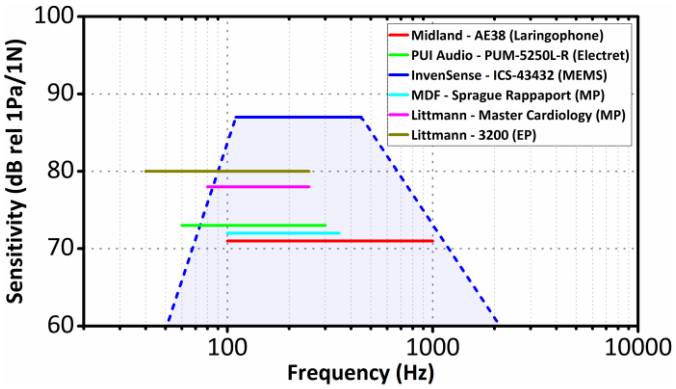

Fig. 6. Sensitivity-bandwidth plot for the comparison of sensors in equivalent noise floor conditions. The vertical position of the line corresponds to the pass-band magnitude of the sensor sensitivity. Moreover, the higher its position along the vertical axis, the higher the signal-to-noise (SNR) provided by the sensor. The horizontal length of the line corresponds to the pass-band bandwidth of the sensor sensitivity.

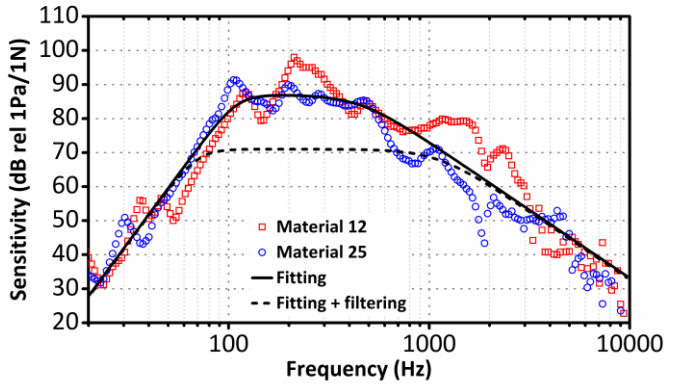

Fig. 7. Detail of the performance of the MEMS sensor (from Fig.5c). The trade-off between sensitivity and bandwidth can be exploited from a system design perspective for different applications. The MEMS sensor inherently implements a high-sensitivity, narrow-band sensing (solid black line). A simple stop-band filter allows tuning the response to a wider bandwidth with different sensitivity settings (dashed black line).

on their mechano-acoustic response, independently of their specific noise floor.

Measuring the responses at a standardized noise floor level enables evaluating the sensors performance and avoiding any fictitious advantage that complex electronic devices (e.g. the Littman 3200) could have thanks to embedded amplification circuitry. In fact, any embedded amplification *within* the transducer would simultaneously increase both the sensor response and its associated noise floor, resulting in a louder sound (which can be useful in some applications) but providing no additional information. Conversely, sensors with low noise floor would be penalized if this is not taken into account during the characterization.

An ESS stimulus was again used to measure the force-to-pressure frequency responses, i.e. the sensitivity of the given sensor, and it is worth repeating that force and pressure signals were firstly acquired synchronously and then post-processed in MATLAB using the ITA-Toolbox [20] according to the ESS method [18], [19], thus leading to the sensitivity of the DUTs (at 50 dB SPL noise floor).

IV. Sensors Responses and Comparison

The sensors characterized in this study are summarized in Table II. The experimental sensitivity extracted as described in Section III is shown in Figure 5. It is worth reminding that material 12 and material 25 (shown in red and blue, respectively) were both employed as standard skins for the sake of comparison.

All responses show an overall band-pass behavior, independently of the type of sensor (either mechanical or electronic). However, large variations can be observed in terms of cut-off frequencies and stop-band slopes. Moreover, resonances of various magnitudes are exhibited by all the sensors throughout the useful bandwidth, complicating the comparison of the experimental responses.

For a better interpretation of data, complex experimental responses were fitted by suitably designed Butterworth band-pass filters. Indeed, this approach allowed to characterize each sensor through a small number of parameters, namely the pass-band magnitude, the cut-off frequencies and the -3dB bandwidth.

These parameters play a twofold role. Firstly, they can ease the reading of the graphs in Figure 5. However, and more importantly, such parameters enable defining a performance metric mimicking the well-known *gain-bandwidth product*. According to this interpretation, the 6 sensors mentioned in Figure 5 are quantitatively compared in Figure 6 in terms of sensitivity-bandwidth.

Since all the DUTs were characterized at an equivalent noise floor, the sensor providing a higher sensitivity (thus higher output and signal-to-noise-ratio) is plotted in the higher part with respect to the vertical axes. Likewise, a wider bandwidth would be depicted as a longer horizontal segment with respect to the frequency axis.

The resulting plot shows a remarkable similarity to the Carnegie Hall musical instruments chart of [21]. This suggests that the proposed approach could be adopted in the future for the quantitative and objective comparison of the performance of devices for lung sound auscultation.

V. Discussion and Future Developments

The methodology discussed so far has some relevant advantages for sensor designers, since it allows one to grasp the capability of sensors in collecting information regardless of the type of device and its inherent noise floor. In this work, different sensors for lung sounds are compared in terms of bandwidth and sensitivity. As far as the former is concerned, the most important message is that the useful band is practically limited to 1 kHz even for state-of-the-art devices. This limitation is entailed by the joint effect of the elasticity of soft tissues and the acoustic coupling between the transducer and the human skin. Considering that most of the devices are based on a vibrating membrane, the range consists of approximately 2 octaves of usable bandwidth (e.g. from 40 Hz to 250 Hz for the Littmann 3200, or from 60 Hz to 300 Hz for the PUI Audio Electret). An exception is represented by the Midland laryngophone providing 3.3 octaves of usable bandwidth (from 100 Hz to 1000 Hz). This agrees to transducer design theory which, considering both the size of the actuator/sensor membrane and the relationship between acoustic wavenumbers and radiation impedance, states that higher efficiency and

constant radiating power (i.e. the so called piston band) is achieved when:

$$ka = \frac{2\pi}{\lambda} a \sim [0.1\,, 2] \qquad (6)$$

where k is the acoustic wavenumber, λ is the acoustic wavelength, and a is the radius of the membrane [22].

While for actuators the piston band can typically extend for almost two decades (which is more than 4.3 octaves), the complex interaction between the *standard skin* and the sensors' membranes, which includes an additional mechano-acoustic interface, further limits the sensing capabilities.

More evidence supporting this interpretation of the data is the good performance of the Midland laryngophone, which directly converts vibrations to electrical signals, without relying on acoustic energy conversion as an intermediate step. This suggests a guideline for designers who want to improve the performance in terms of useful bandwidth, namely to minimize the number of energy conversions performed by the sensor. This could be for example achieved eliminating one mechano-acoustic interface, i.e. sensing vibrations and accelerations directly, which could mitigate the intrinsic limitations due to multiple interfaces and coupling. In this case the expected bandwidth could be as large as 4 octaves.

As far as sensitivity is concerned, experimental results show how modern devices based on digital MEMS (e.g. the InvenSense ICS-43432) can outperform other candidates by almost 15 dB. Interestingly, from a technical point of view, this MEMS device is more similar to an accelerometer than to a microphone. As a consequence, it would be expected to offer a broader usable bandwidth.

The fact that the measured bandwidth for this transducer seems to disagree with what stated above is not a contradiction or a limitation of the technology but, on the contrary, the result of a mature design decision. In fact, if some sensitivity gain reduction is accepted, a significant bandwidth extension could be achieved. This idea is suggested in Figure 7 by plotting on the same graph two fitting curves, reflecting two different levels of target sensitivity.

Moving on with the same rationale, the sensitivity-bandwidth metric could be reinterpreted to provide a region of "maximum absolute ratings". This idea is sketched in Figure 6 by using the MEMS transducer as an example. In practice the blue area subtends the set of working points allowed by the MEMS transducer, so that the designer can adjust the trade-off between sensitivity and bandwidth according to the system requirements. Such flexibility is another suggested guideline for the designer. For instance, pulmonary sounds characterized by a very large bandwidth could be acquired with a relatively low sensitivity to have a broad overview of possible lung implications. On the other hand, the lung sounds showing peculiar narrow band features could be acquired with significantly higher sensitivity to maximize the chance of detection of specific diseases [4]–[6].

VI. Conclusion

The first part of this study is devoted to the search and characterization of synthetic materials suitable to mimic the vibro-acoustical properties of human soft tissues and become a reference benchmark which could be referred as *standard skin*. A large set of multi-layered materials typically used as acoustic panels was considered. Two materials were identified as best candidates to represent the standard skin, namely Material 25 (SUPERGRAN, mm. 5) and Material 12 (SUPERFINE, mm. 8+3). The worldwide availability of these acoustic panels paves the ways to reproducible measurements and fair comparison.

Then, in the second part of this work, the *standard skins* were used to benchmark a large set of sensors suitable to the acquisition of lung sounds. Different types of transducers were assessed, namely laryngophone, electret microphone, digital MEMS microphone, mechanical phonendoscope and electronic phonendoscope.

All sensors were compared in terms of sensitivity, in equivalent noise floor condition. The new interpretation of experimental results led to the concepts of normalized sensitivity and equivalent usable bandwidth. These concepts, in

TABLE III
Standard Skin Candidate Materials

Material	Name	MAPE	MSE (×10^6)
1	MANTOBIT mm. 3+5+3	9.69	675.22
2	MANTOPHON BIT mm. 5+4+5	18.58	2935.71
3	MANTOPHON Superbit mm. 8+4	11.04	601.94
4	MICROMANT mm. 5	36.25	28976.93
5	MANTOPHON BIT mm. 5+3	11.54	970.12
6	MANTOPHON BIT mm. 5+4	13.37	1245.76
7	POLYMANT C/33 CL1 mm. 5	10.56	590.69
8	MANTOSOL mm. 5+4+3	10.16	658.66
9	MANTOPHON PLUS mm. 3+0.5+8	12.14	866.98
10	MANTOPHON PB CL1 mm. 3+0.5+3	15.38	2145.45
11	MANTOPHON PB mm. 3+0.5+3	12.45	1030.98
12	SUPERFINE mm. 8+3	9.61	460.76
13	MANTOPHON ECOFIRE mm. 3+3+3	21.33	19786.44
14	MICROGIPS mm. 12.5+10	24.06	11651.80
15	BLUEBIT mm. 3+4	11.57	651.79
16	POLYMIX PB CL.1 Riv mm. 3+0.5+20	17.08	3379.53
17	POLYWALL PB CL.1 Riv mm. 20+0.5+20	18.85	2772.78
18	MANTOPHON ECOLIGHT mm. 3+3+3	24.93	7361.26
19	MANTOPHON BIT mm. 5+4+5	17.86	3485.01
20	MANTOPHON ECOFINE mm. 3+3+3	18.38	2637.94
21	MANTOPHON PLUS mm. 3+0.5+8	14.88	1444.84
22	EUROWOOD PB mm. 12+0.35+19	17.72	2564.72
23	MANTOPHON PB evolution mm. 4+0.5+4	25.44	41416.83
24	MANTOPHON Light mm. 3+0.35+3	14.21	1183.67
25	SUPERGRAN mm. 5	7.56	332.80

turn, allow to compare, classify and rank sensors of different nature. Six devices for dorsum auscultation were analyzed and discussed in detail. Finally, important design guidelines were devised by our new perspective.

In particular, the presence of a vibrating membrane seems to limit the trade-off between bandwidth and sensitivity, thus suggesting to push the research towards "solid state transducers" like accelerometers and MEMS microphone. On the basis of recent studies available in literature, we believe that new high-performance sensors for the acquisition of lung sounds could represent one of the key technologies for the automatic detection of pulmonary diseases.

APPENDIX A

Table III lists all the candidate materials for *standard skin* tested in this study, along with the related evaluation metrics described in Section III (i.e. the MAPE and MSE of materials apparent mass with respect to the real skin apparent mass). All the candidate materials are readily available off-the-shelf multi-layered panels with applications in the field of building acoustics produced by Polymaxitalia [14].

REFERENCES

[1] A. A. Shkel and E. S. Kim, "Continuous Health Monitoring With Resonant-Microphone-Array-Based Wearable Stethoscope," *IEEE Sens. J.*, vol. 19, no. 12, pp. 4629–4638, 2019, doi: 10.1109/JSEN.2019.2900713.

[2] A. B. Kambhampati and B. Ramkumar, "Automatic Detection and Classification of Systolic and Diastolic Profiles of PCG Corrupted Due to Limitations of Electronic Stethoscope Recording," *IEEE Sens. J.*, vol. 21, no. 4, pp. 5292–5302, 2021, doi: 10.1109/JSEN.2020.3028373.

[3] V. T. Tran and W. H. Tsai, "Stethoscope-Sensed Speech and Breath-Sounds for Person Identification with Sparse Training Data," *IEEE Sens. J.*, vol. 20, no. 2, pp. 848–859, 2020, doi: 10.1109/JSEN.2019.2945364.

[4] A. Manfredi *et al.*, "Diagnostic accuracy of a velcro sound detector (VECTOR) for interstitial lung disease in rheumatoid arthritis patients: The InSPIRAtE validation study (INterStitial pneumonia in rheumatoid ArThritis with an electronic device)," *BMC Pulm. Med.*, vol. 19, no. 1, pp. 1–6, 2019, doi: 10.1186/s12890-019-0875-x.

[5] F. Pancaldi *et al.*, "Analysis of pulmonary sounds for the diagnosis of interstitial lung diseases secondary to rheumatoid arthritis," *Comput. Biol. Med.*, vol. 96, pp. 91–97, 2018, doi: 10.1016/j.compbiomed.2018.03.006.

[6] A. Manfredi *et al.*, "Usefulness of Digital Velcro Crackles Detection in Identification of Interstitial Lung Disease in Patients With Connective Tissue Diseases," *Arch. Rheumatol.*, Jun. 2020, doi: 10.46497/ArchRheumatol.2021.7975.

[7] P. Y. Ertel, M. Lawrence, R. K. Brown, and A. M. Stern, "Transmission and Filtration Patterns," *Circulation*, vol. 34, no. November, pp. 899–909, 1966.

[8] H. Pasterkamp, S. S. Kraman, and G. R. Wodicka, "Respiratory Sounds," *Am. J. Respir. Crit. Care Med.*, vol. 156, no. 3, pp. 974–987, Sep. 1997, doi: 10.1164/ajrccm.156.3.9701115.

[9] P. Korhonen, "Frequency response measurements on commercially available stethoscopes," *Med. Biol. Eng. Comput.*, vol. 34, no. SUPPL. 1, pp. 91–92, 1996.

[10] V. I. Korenbaum, A. A. Tagil'Tsev, A. I. D'Yachenko, and A. E. Kostiv, "Comparison of the characteristics of different types of acoustic sensors when recording respiratory noises on the surface of the human chest," *Acoust. Phys.*, vol. 59, no. 4, pp. 474–481, 2013, doi: 10.1134/S1063771013040088.

[11] A. A. Alanazi, S. R. Atcherson, C. A. Franklin, and M. F. Bryan, "Frequency Responses of Conventional and Amplified Stethoscopes for Measuring Heart Sounds.," *Saudi J. Med. Med. Sci.*, vol. 8, no. 2, pp. 112–117, 2020, doi: 10.4103/sjmms.sjmms_118_19.

[12] M. Sarkar, I. Madabhavi, N. Niranjan, and M. Dogra, "Auscultation of the respiratory system," *Ann. Thorac. Med.*, vol. 10, no. 3, pp. 158–168, 2015, doi: 10.4103/1817-1737.160831.

[13] V. Korenbaum and A. Shiryaev, "The features of sound propagation through human lungs, revealed by transmission sounding with phase manipulated acoustic signal of 80–1000 Hz frequency band," *J. Acoust. Soc. Am.*, vol. 137, no. 4, pp. 2424–2424, 2015, doi: 10.1121/1.4920840.

[14] "POLYMAX ITALIA | Acoustic Insulation Technology." https://polymaxitalia.it/ (accessed Aug. 02, 2021).

[15] T. D. Mast, "Empirical relationships between acoustic parameters in human soft tissues," *Acoust. Res. Lett. Online*, vol. 1, no. 2000, pp. 37–42, 2000, doi: 10.1121/1.1336896.

[16] N. J. Mansfield, "Impedance methods (apparent mass, driving point mechanical impedance and absorbed power) for assessment of the biomechanical response of the seated person to whole-body vibration," *Ind. Health*, vol. 43, no. 3, pp. 378–389, 2005, doi: 10.2486/indhealth.43.378.

[17] Polymaxitalia, "POLYMAX ITALIA : Acoustic Insulation Technology," *03/07/2021*. https://polymaxitalia.it/ (accessed Aug. 02, 2021).

[18] A. Farina, "Simultaneous measurement of impulse response and distortion with a swept-sine technique," *Present. 108th AES Conv. Paris, Fr.*, 2000, doi: 10.1109/ASPAA.1999.810884.

[19] A. Farina, "Advancements in impulse response measurements by sine sweeps," *Present. 122nd AES Conv. Vienna, Austria*, 2007.

[20] M. Berzborn, R. Bomhardt, J. Klein, J. G. Richter, and M. Vorländer, "The ITA-Toolbox : An Open Source MATLAB Toolbox for Acoustic Measurements and Signal Processing," *Ger. Annu. Conf. Acoust.*, pp. 222–225, 2017, [Online]. Available: http://www.ita-toolbox.org/publications/ITA-Toolbox_paper2017.pdf.

[21] T. Rossing, *Springer Handbook of Acoustics*. New York, NY: Springer New York, 2014.

[22] J. Eargle, *Loudspeaker Handbook*. Boston, MA: Springer US, 2003.

Paolo La Torraca graduated in Computer Engineering (cum Laude) in 2015 at the Politecnico di Milano, Italy. He received his Ph.D. degree in Information and Comunication Technology (ICT) at the University of Modena e Reggio Emilia, Italy. He is now Research Fellow at the University of Modena and Reggio Emilia. He works in the fields of electronics and nanomaterials. His research interests include the study, characterization and simulation of novel electro-mechanical and electro-acoustic transducers.

Ludovico Ausiello completed his integrated masters degree in electronics at University of Bologna in 2004, and achieved his European PhD in 2009 from the same institution. He worked as a Research Associate with Prof Angelo Farina and MagnetiMarelli S.p.A between 2009 and 2012, where he developed smart acoustic sensors for engine control systems and a patent to perform acoustic recognition of different types of fuel from combustion's noise. Between 2012 and 2018 he worked in the loudspeaker industry, being System Engineer at Harman, Senior Acoustic Engineer at Tannoy, and blue-sky researcher at PSS. He joined the academic environment again in 2018, when he became Senior Lecturer in acoustics and audio engineering at Solent University (Southampton), and then moved to University of Portsmouth to teach analog electronics in 2021. Member of the Institute of Acoustics and of the AES, he's also a member of the Higher Education Academy, undertaking both scientific and pedagogical research, with a particular interest in musical acoustics and transducer design.

Giorgio Zucchi graduated in Management Engineering at the University of Modena and Reggio Emilia, Italy, 2018. He is currently working toward a Ph.D. degree in Labour, Development and Innovation at the Università di Modena e Reggio Emilia, Italy. His research interest includes the study and creation of mathematical models and meta-heuristic algorithms to develop optimization methods, with particular attention to the Personnel Scheduling Problem and Vehicle Routing Problem.

Angelo Farina was born in 1958. He got his Master Degree in civil engineering in December 1982 at the University of Bologna (IT) with a thesis on the acoustics and vibrations inside a tractor cab. In 1987 he got a PhD in Technical Physics at the University of Bologna with at thesis on experimental assessment of concert hall acoustics. He was a full-time researcher since 1st November 1986 at the University of Bologna, and since 1st march 1992 at the University of Parma, where he became Associate Professor on 1st November 1998 and Full Professor of Environmental Applied Physics since 1st May 2005, where he has the chairs of Applied Acoustics and Environmental Technical Physics. During his academic career Angelo worked in several fields of Applied Acoustics, including noise and vibration, concert hall acoustics, simulation software and advanced measurement systems. In the last 10 years Angelo focused mostly on applications involving massive microphone and loudspeaker arrays. In 2008 Angelo Farina was awarded with the AES fellowship for his pioneering work on electroacoustic measurements based on exponential sine sweeps. Angelo is author of more than 300 scientific papers and three widely-employed software packages (Ramsete, Aurora Plugins, DISIA).

Fabrizio Pancaldi (M'04) was born in Modena, Italy, in 1978. He received the Dr. Eng. degree in electronic engineering (cum Laude) in 2002 and the Ph.D. degree in information engineering in 2006, both from the University of Modena and Reggio Emilia, Italy. Since 2006 he has been Assistant Professor at the University of Modena and Reggio Emilia. He works in the broad field of digital signal processing with particular emphasis to biomedical engineering, wireless and powerline communications, indoor localization and condition monitoring of machinery.